

# Forward Modelling the O3a GW transient mass distributions with BPASS by varying compact remnant mass and SNe kick prescriptions

Sohan Ghodla<sup>1</sup>, Wouter G. J. van Zeist<sup>1</sup>, J. J. Eldridge<sup>★1</sup>, Héloïse F. Stevance<sup>1</sup>, Elizabeth R. Stanway<sup>2</sup>

<sup>1</sup>*Department of Physics, University of Auckland, Private Bag 92019, Auckland, New Zealand*

<sup>2</sup>*Department of Physics, University of Warwick, Gibbet Hill Road, Coventry, CV4 7AL, UK*

Accepted XXX. Received YYY; in original form ZZZ

## ABSTRACT

We present forward modelling from the BPASS code suite of the population of observed gravitational wave (GW) transients reported by the LIGO/VIRGO consortium (LVC) during the first half of their third observing run (O3a). Specifically, we predict the expected chirp mass and mass ratio distributions for GW transients, taking account of detector sensitivity to determine how many events should have been detected by the current detector network in O3a. We investigate how these predictions change by alternating between four different remnant mass estimation schemes and two supernovae (SNe) kick prescriptions. We find that none of the model populations resulting from these variations accurately match the whole O3a GW transient catalog. However, agreement from some models to part of the catalog suggests ways to achieve a more complete fit. These include reducing the number of low mass black holes (BHs) close to the mass gap, while also increasing the number of higher mass BHs below the pair-instability SN limit. Finally, we find that the interaction between the value of the remnant mass from a stellar model and the choice of SN kick is complex and different kick prescriptions may be required depending on whether a neutron star or BH is formed.

**Key words:** stars: evolution – binaries: general – supernovae: general – methods: numerical

## 1 INTRODUCTION

In the span of only half a decade, the detection of GW transients has become almost routine. After LVC O3a, there are now 50 known GW transients events with a false-alarm rate below  $2 \text{ yr}^{-1}$  (Abbott et al. 2020a). Each event in itself reveals much about the evolution of binary stars (e.g. for individual studies see Abbott et al. (2016, 2017, 2020b) and for evolutionary implications for binaries, see Eldridge & Stanway (2016); Belczynski et al. (2016); Stevenson et al. (2017); Mapelli et al. (2017); Vigna-Gómez et al. (2018); Eldridge et al. (2019); Lipunov et al. (2021); Broekgaarden et al. (2021) and references therein). However with a growing understanding of the distribution of masses, we are now beginning to constrain the population of GW transients both through parametric models (e.g. Abbott et al. 2019; Abbott et al. 2020a) or using the technique of population synthesis to understand the physical process of stellar evolution that gives rise to the mass distribution (e.g. Belczynski et al. (2008); Stevenson et al. (2017); Eldridge et al. (2017); Giacobbo et al. (2018) and references therein).

While binary population synthesis is a powerful tool, there are many uncertainties in the physics incorporated in these models (e.g. De Marco & Izzard 2017) as well as in the prescriptions used

to model the star formation history and chemical evolution of the Universe (Belczynski et al. 2016; Mapelli et al. 2017; Chruslinska et al. 2019; Tang et al. 2020; Boco et al. 2021; Broekgaarden et al. 2021). In particular, apart from the uncertainties in evolution of massive single stars (eg. mass-loss rate, rotation, overshooting etc.) the understanding of the mass-transfer and common envelope phase in binaries is also incomplete (eg., Ivanova et al. 2013 and references therein). In addition, Fishbach & Kalogera (2021) found evidence of the delay time distribution mostly lying within 0–4.5 Gyrs although a subset of GW mergers has also been found to come from very long time delays (eg., Eldridge & Stanway 2016; Mapelli et al. 2017). As such, the wide distribution of possible delay time intervals between the formation of the progenitor stellar binary of a GW transient and the inspiral event introduces sensitivity to past star formation conditions. Another required assumption is the remnant mass prescription used to determine the compact remnant mass once the stellar model reaches its final state, which often does not proceed all the way to core-collapse for numerical reasons. To this end, several remnant mass prescriptions with different features also exist in the literature, e.g. see, Patton & Sukhbold (2020).

In this letter, we utilize BPASS (Binary Population and Spectral Synthesis) code results to forward model the population of GW transients resulting from their underlying stellar population up till their chirp event, specifically predicting the distribution of expected

★ j.eldridge@auckland.ac.nz

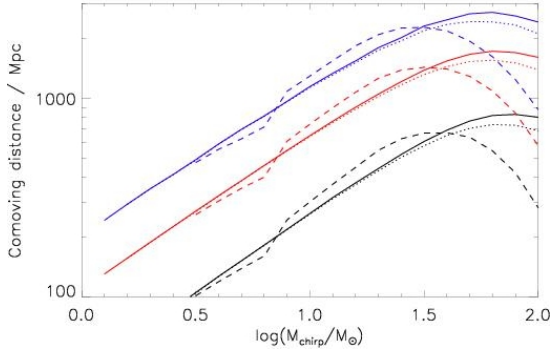


**Figure 1.** The detection distance versus chirp mass as a function of detection probability and mass ratio. The solid, dotted and dashed lines represent the mass ratio values  $q = 1$ ,  $q = 0.5$  and  $q = 0.1$ . The black lines are for a detection probability of 0.9, red 0.5 and blue 0.1.

chirp masses and mass ratios for them during LVC O3a. Section 2 outlines the numerical model, highlighting the differences between this and earlier *BPASS* work. Specifically, here we vary two key uncertainties in our analysis, (i) the nature of the kick that remnants receive while undergoing a SN explosion and (ii) the prescription for calculating the resulting remnant masses. Section 3 presents our results on the number of expected detections and the predicted GW transient object mass distribution. We then compare these to the LVC O3a catalog (Abbott et al. 2020a) to see which of the prescriptions produce a mass distribution that closely matches their results, presenting discussion and concluding remarks in section 4.

## 2 METHODS AND PRESCRIPTIONS, SIMULATIONS AND OBSERVATIONS

Our aim here is to forward model the population of GW transients that may have been detected in O3a, making predictions independent of the O3a observations, and explore some of the stellar evolutionary uncertainties that might impact these results. We use four different schemes to estimate the remnant masses resulting from stellar evolution and two different kicks to investigate how they interact to affect the populations of the predicted GW mergers.

### 2.1 Population synthesis

We use *BPASS* v2.2.1 stellar models (Eldridge et al. 2017; Stanway & Eldridge 2018) and build upon our earlier work on predicting the GW transient rates. We refer the reader to those papers for full details of our model and method (Eldridge & Stanway 2016; Eldridge et al. 2019; Tang et al. 2020). We use the same underlying model of the cosmological star formation history and metallicity evolution as in Eldridge et al. (2019). However, two aspects of our previous population synthesis have been improved.

Firstly, we have updated the treatment of rejuvenation during mass transfer onto the secondary stars. *BPASS* has two principal sets of models: *primary models* where the more massive star’s full structure is computed in detail and the secondary’s evolution is approximated using the equations of Hurley et al. (2000); and *secondary models* where the secondary is evolved in detail as either a single star or a star in orbit around a compact object – depending on the outcome of the first SN. Many different primaries map onto the same secondary model. As a result, in earlier *BPASS* calculations we used an average rejuvenation age (i.e. time step at which mass transfer leads to rotational mixing, causing the accretor to become chemically homogeneous eg., Maeder 1987) for each secondary model. In this work, we use a distribution of rejuvenation ages for

each secondary model. This has the effect of smoothing out our delay time distribution for transient events driven by GW emission.

Secondly, we now compute the GW merger time by calculating the orbital evolution in full as outlined by Peters (1964) rather than by simple interpolation between the two analytic forms for circular and highly eccentric orbits. This is motivated by the fact that many of the orbits lie in the mid-range between circular and eccentric after the second supernova, and the updated calculations offer a more accurate prediction of the merger times.

### 2.2 Detection horizons

Detection of predicted mergers will depend on instrumental and alignment effects. Suites of codes to evaluate this do exist, such as *LALSUITE* (LIGO Scientific Collaboration 2018), but we implement our own Python package to do this because of our specific focus on population synthesis. The package *RIRORIRO*<sup>1</sup> has been created with the aim of determining the fraction of predicted GW transients that can be detected (van Zeist et al. 2021). Currently, it only deals with GW transients caused by the merger of NSNS, NS-BH, and BHBH. In the future, we plan to extend its scope to all areas of GW population and the resulting GW spectral synthesis.

For each chirp mass and mass ratio pair *RIRORIRO* creates a synthetic merger gravitational waveform (including inspiral and ringdown phases). The effects of source orientation and distance are then taken into account to calculate an effective detection volume and the evolution of detection fraction of these events with luminosity distance. Our calculations span from 1 Mpc to 10 Gpc in steps of 0.1 dex. The package is inspired from Buskirk & Babiuc-Hamilton (2019) who created a *MATHEMATICA* routine to calculate the expected GW waveform for a GW transient event. They used the results of Huerta et al. (2017) to model the inspiral and ringdown emission. We use the same methods they outline as well as using information from the *FINDCHIRP* algorithm (Allen et al. 2012) to improve our modeling of the inspiral waveform and calculation of the signal-to-noise ratio (SNR). It is often difficult to match the inspiral and ringdown waveforms and we switch between them when the frequency and time derivative are closest between the two models.

For each resultant waveform, we use the method of Barrett et al. (2018) to calculate the SNR of the merger model at a given redshift using the corresponding luminosity distance and redshifting the waveform. We subsequently calculate a total SNR assuming a triple-detection by combining the SNR calculated for the LIGO Hanford, LIGO Livingston, and VIRGO detectors during O3 in quadrature. We also calculate the average expected SNR of a GW observation with a single, non-specific detector operating. These SNR values assumed optimal alignment of detector and source. To take into account the effect of arbitrary orientation we multiplied these with a projection function (Finn 1996; Belczynski et al. 2013, 2014), giving a probability distribution of the expected SNR and the probability that this would exceed the commonly-used detectability threshold value of 8, i.e. the detection probability. The variation in the detection probability of a GW transient depending on the chirp mass, mass ratio, and distance of the binary is illustrated in Fig. 1. For each chirp mass, there is a maximum distance beyond which no mergers can be detected but there is a smoothly decreasing detection probability up to this horizon. Higher chirp masses can be detected to larger distances. However, at the highest chirp masses a hard upper limit is introduced due to the decreasing maximum frequency of

<sup>1</sup> A *riroriro* is a bird native to Aotearoa New Zealand that is frequently heard but seldom seen.

these mergers. This upper limit is most sensitive to the mass ratio, as shown in Fig. 1, and the lowest mass ratio has a significantly lower maximum chirp mass for the peak comoving distance to the source. We combine the detection probabilities as a function of chirp mass, mass ratio and distance with the population statistics from BPASS, which dictate the frequency with which systems of such parameters form, to create a forward model for the LVC detection rates. We integrate the rates in events per year per unit volume over the observable Universe to obtain rates in events per year. We use the method of Hogg (1999) to convert the luminosity distances used in the previous steps to comoving distances which are employed in the volume calculations<sup>2</sup>. We reduce our rates by a factor of (177.3 days / 365.25 days) to account for the elapsed duration during O3a where at least one detector was active and taking data.

### 2.3 Remnant mass estimates and supernova kick velocities

Within BPASS the standard method of calculating remnant masses at the end of stellar evolution for massive stars is to compare the binding energy of the stellar envelope to the typical SN explosion energy of  $10^{51}$  ergs. The ejecta mass is considered to be the amount of mass with this much binding energy, removed from the star, and the remainder goes into the remnant mass (Eldridge & Tout 2004). Here we refer to this method as our *Standard* remnant mass scheme. However, to explore the effect of varying the remnant mass prescription on our predictions, we look into three other schemes.

The first two are referred as *AlwaysNS* and  $M_{\text{CO,final}}$  and are near the extremes of what we might expect for remnant masses, although some stars may completely collapse into a BH. In *AlwaysNS*, motivated by the Chandrasekhar mass limit, we force all the models to form a neutron star (NS) of  $1.4 M_{\odot}$  at core-collapse. Although remnants with a range of NS mass could form, we have to limit the number of allowed remnant masses because of BPASS using detailed stellar evolution models and producing a fine grid of such models would require significant computational time (Eldridge et al. 2008, Eldridge et al. 2017). Our primary focus here remains the BH mass distribution, so *AlwaysNS* assumption produces a lower limit on the distribution of chirp masses of our model GW transients. On the other hand in  $M_{\text{CO,final}}$  the final carbon-oxygen core mass of the progenitor model is set equal to the remnant mass (i.e. only the hydrogen/helium envelope will be ejected, independent of SN energy). This will lead to the maximum mass distribution for GW transient chirp masses. Both of these assumptions are unphysical but permit us to explore the limits of our predictions.

Finally, we compare these to a commonly-used rapid synthesis scheme from Fryer et al. (2012), here referred as *FryerRapid*. This scheme gives a remnant mass that depends on  $M_{\text{CO,final}}$  (and partly on  $M_{\text{final}}$ ) of the stellar model. An interesting feature is that it predicts a mass-gap in the BH mass distribution with no BHs less massive than  $5 M_{\odot}$ . Consequently, using the *FryerRapid* scheme allows us to determine the impact of allowing for a mass-gap. Finally in addition to using the above remnant mass distributions we also use two different SN kick schemes namely the Hobbs et al. (2005) and Bray & Eldridge (2018) kick velocity relations. The former is described by a Maxwell-Boltzmann distribution with 1 dimensional root mean square speed of  $265 \text{ km s}^{-1}$  while the latter depends strongly by construction on the ejecta and remnant masses and thus we expect the kick and remnant mass distributions to interact in a complex and non-linear way.

**Table 1.** Predicted number of observable detections during O3a for the three expected mergers types, employing various methods for calculating SN kicks and remnant masses. Rates in parenthesis are intrinsic merger rates (in units of events  $\text{Gpc}^{-3} \text{ yr}^{-1}$ ) calculated before the consideration of detection probabilities. Last row states the LVC O3a observed and intrinsic rates (Abbott et al. 2020a, 2021).

Kick	Remnant	NSNS	BHNS	BHBH
Hobbs	Standard	2.7 (208)	7.0 (131)	25 (31)
Hobbs	$M_{\text{CO, final}}$	0.86 (43)	26 (417)	233 (873)
Hobbs	FryerRapid	2.1 (176)	15 (208)	95 (169)
Hobbs	AlwaysNS	2.7 (223)	0.21 (8.7)	0.0
Bray	Standard	9.5 (745)	7.4 (180)	15 (13)
Bray	$M_{\text{CO, final}}$	3.1 (179)	24 (498)	118 (569)
Bray	FryerRapid	7.6 (677)	8.9 (157)	36 (70)
Bray	AlwaysNS	8.0 (708)	1.1 (48)	0.0
<b>LVC O3a</b>		$1 \pm 1$	$2 \pm 1.4$	$36 \pm 6$
<b>Intrinsic [<math>\text{Gpc}^{-3} \text{ yr}^{-1}</math>]</b>		$(320^{+490}_{-240})$	$(\leq 610)$	$(23.9^{+14.3}_{-8.6})$

## 3 RESULTS

### 3.1 Rates

Our results shown in Table 1 (also see Fig. A5 in the Appendix), presents the expected number of events that should have been detected in O3a under each set of prescriptions. On considering the number of expected events (Table 1, Fig. A5) resulting from each remnant mass and SN kick prescription in the light of O3a detection rate data, we observe patterns with interesting implications:

(i) The *Bray kick* consistently give a high NSNS and a low BHBH merger rate, when compared to the *Hobbs kick*. The strength of these differences varies between the remnant mass schemes but the general trend holds except under the unrealistic  $M_{\text{CO,final}}$  scheme. One explanation could be that in the *Bray kick*, the kick velocity is inversely proportional to the remnant mass. Thus massive BHs receive weaker kicks and so have less eccentric orbits, longer merger times and a lower BHBH merger rate. As discussed in Bray & Eldridge (2018), as the accuracy of the observationally measured merger rate density improves, it will be possible to use this as a constraint in combination with the neutron star velocity distribution to refine the values of the *Bray kick* prescription.

(ii) In  $M_{\text{CO,final}}$ , the BHBH and BHNS merger rates are significantly higher than those observed in O3a implying that stellar remnants must be consistently less massive than the final CO core mass of their progenitors. Fig. A3 (discussed later) also demonstrates this bias of  $M_{\text{CO,final}}$  toward the higher mass remnants.

(iii) All our schemes overpredict the BHNS merger rate, except the *AlwaysNS*, suggesting that the mass distribution at the change over from NSs to BHs is complex and requires further study.

(iv) *Standard* remnant mass scheme underpredicts the number of expected BHBH mergers, more so using the *Bray kick*. This implies that isolated binary evolution will not be the only source of these mergers, with a fraction likely arising from dynamical pathways.

(v) The BHBH O3a merger rate is exactly reproduced by *Bray kick* + *FryerRapid* remnant scheme. However, this also produces too many mergers involving NSs. Moreover, it also implies that binary BHs formation with the dynamical channels are very rare.

(vi) The *AlwaysNS* scheme does have some BHNS mergers despite no BHs being formed in core-collapse. These BHs are the result of the subsequent accretion-induced collapse of already formed NS from its still evolving companion and give an indication of the relative importance of such a channel compared to normal BHNS mergers where one of the BHs is formed directly at core-collapse.

<sup>2</sup> We assume a standard  $\Lambda$ CDM cosmology with  $H_0 = 100h \text{ km s}^{-1} \text{ Mpc}^{-1}$  with  $h = 0.696$ ,  $\Omega_M = 0.286$ ,  $\Omega_\Lambda = 0.714$

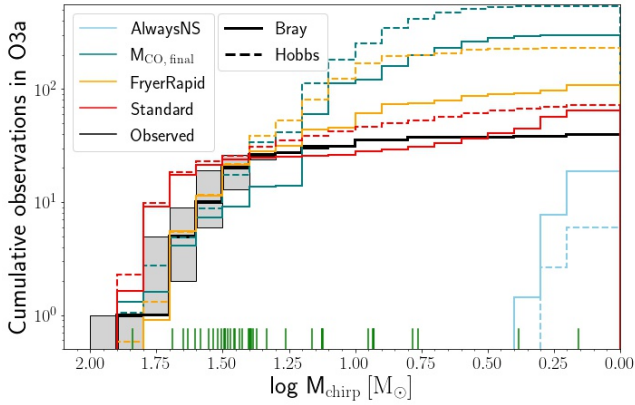


**Figure 2.** The Chirp mass distributions of events observed by LVC O3a (black line) and those predicted by our model populations for the same duration of observation. The green ticks show the observed values of  $M_{\text{chirp}}$  and the solid grey area represents the uncertainty between the upper and lower  $M_{\text{chirp}}$  bounds for these observed events (Abbott et al. 2020a). The black curve is the cumulative observed events over the best estimated  $M_{\text{chirp}}$  range. Solid lines represent *Bray* kick while dashed lines *Hobbs* kick.

### 3.2 Chirp mass distribution

Using rates alone is a limited approach to constrain the models. We must consider the number of events expected in chirp mass and mass ratio space as well. To this end, we first consider the predicted chirp mass distribution of our model GW transient populations. Fig. 2 shows the cumulative number of GW transients versus chirp mass from the high-mass end of the chirp mass distribution. We see that most of the model distributions match observations at high-mass down to  $\log 1.4$  (i.e.  $\sim 25 M_{\odot}$ ) well, although the *Standard* scheme (both kicks) tends to predict a higher count of massive mergers than observed. Below  $25 M_{\odot}$ , the distributions diverge significantly, with most schemes predicting more GW transients of lower chirp mass than is observed. In particular, at the lowest chirp masses (spanning BHNS/NSNS mergers) we see that populations arising from *Bray* kick have an excess of systems. From this figure however, it is possible to identify the schemes that closely match the observed cumulative events count over the  $M_{\text{chirp}}$  range.

We now further the analysis by comparing the GW transient distributions in chirp mass and mass ratio space. Fig. 3, shows the schemes that offer a closest fit to the total event rates in Table 1 (i.e., *Standard* + *Hobbs* kick and *FryerRapid* + *Bray* kick). While the *Standard* scheme spans nearly all combinations of remnant mass, however, in the *FryerRapid* scheme the mass gap (Bailyn et al. 1998; Özel et al. 2010) becomes apparent due to a clear lack of BH systems near the BHNS/BHBH dividing lines. Also in Fig. A1 in the Appendix, the *Standard* + *Bray* kick scheme underpredicts the BHBH and over-predicts the NSNS events. The *FryerRapid* + *Hobbs* kick scheme in Fig. A2 also fails to provide a reliable prediction for the total events as a function of chirp mass.

At  $\log(M_{\text{chirp}}/M_{\odot})$  near 0.7 (i.e.  $\sim 5 M_{\odot}$ ) - close to the mass-gap end, - the *Standard* scheme (with both kicks) overpredicts the number of expected mergers. The *FryerRapid* results in Fig. 3 do achieve the correct peak in chirp mass. However, it predicts a second, much larger peak at further lower chirp masses and a very strong BHNS peak. If we now compare the distribution of the observed GW transients to our forward-model predictions, we find that the small number statistics still limit a meaningful comparison. In Fig. 3 the peak in predicted and observed number of events lie at similar but not identical masses. This suggests a need for further investigation

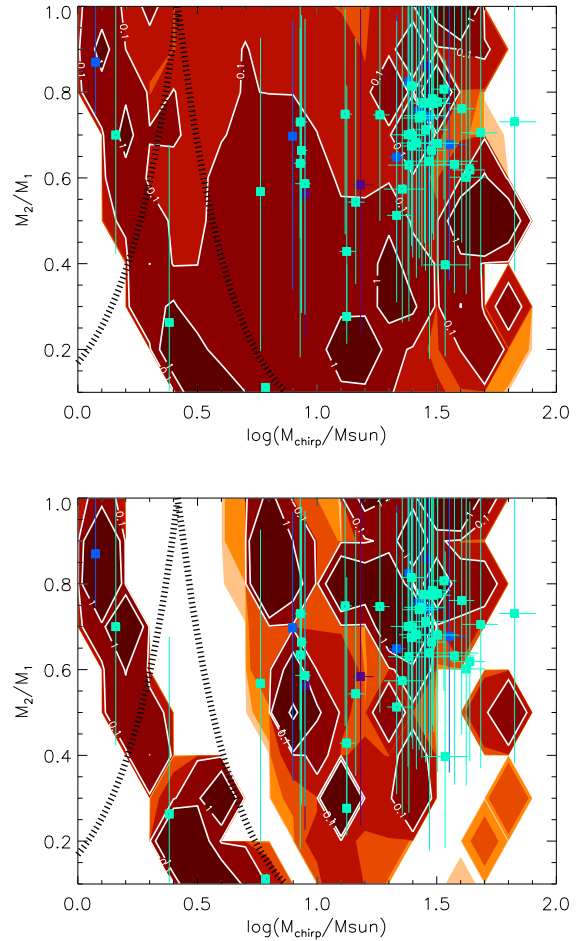


**Figure 3.** Contour plots of the expected distributions of detected events in O3a in  $M_{\text{chirp}}$  and mass ratio space. The upper panel shows the *Hobbs* kick and the *Standard* remnant mass scheme, the lower panel shows the *Bray* kick and the *FryerRapid* remnant mass scheme. Darker contours represent a higher probability. The black dotted line distinguishes the regions where mergers occur with component masses both either below  $3M_{\odot}$ , one above and one below or both above  $3M_{\odot}$  (i.e., the expected regions of NSNS, BHNS, and BHBH mergers). The dark blue symbols are the events from O1, the blue symbols are from O2, and the cyan symbols are from O3a.

at the upper end of the BH mass distribution, close to the mass range of pair-instability SNe (e.g. Woosley 2017; Stevenson et al. 2019).

## 4 DISCUSSION & CONCLUSIONS

In this letter, we have presented theoretical predictions of the expected number of events (and their distribution in chirp mass and mass ratio space) detected within *BPASS* under LVC O3a sensitivity criteria. We find that none of the remnant mass schemes and SN kick combinations we presented fully describe the observed population of GW transients in the O3a catalog. Although most population models do reasonably well in reproducing the chirp mass distribution at masses above  $\sim 25 M_{\odot}$  but diverge considerably at lower masses. Our results suggest that the *Standard* + *Hobbs* kick scheme performs the best overall but requires modification at the upper and lower ends of the chirp mass distribution. The values of the most massive chirp masses predicted by this scheme need to be reduced by 0.1-0.2 dex, while the mass-gap needs to be included in some form at the lower mass end of the BH mass distribution. However, since the event GW190814 (Abbott et al. 2020b) is not predicted

in the *FryerRapid* scheme, this suggests that a prescription making low mass BHs significantly rarer, rather than preventing them from forming entirely within the mass-gap, may be required (also see, Zevin et al. 2020). The *Standard + Hobbs kick* somewhat underpredicts the observed BHBH event rate in Table 1, but these are the outcome of isolated binary evolution only (eg. see, Zevin et al. 2021). Moreover, our models do not yet allow for tidally-induced chemical homogeneous evolution which (as pointed out, see de Mink et al. 2009; de Mink & Mandel 2016; Marchant et al. 2016) could result in a higher BHBH merger rate. Additionally, BHBH mergers could also come from dynamical channels in young stellar or globular clusters (e.g., Kulkarni et al. 1993; Portegies Zwart & McMillan 2000) or at the disks of active galactic nuclei (e.g., McKernan et al. 2012) and some BHBH systems could be of primordial origin, arising in the early Universe (Carr & Hawking 1974). Tang et al. (2020) found that the GW transient rates involving BHs are highly dependent on the rate of chemical enrichment of the Universe. According to their findings, the number of BHNS and BHBH mergers can be reduced by altering the cosmic metallicity evolution. However, a much faster rapid enrichment would be required for our highest predicted rates to match those observed in O3a.

To conclude, we find some of our model populations produce a reasonable agreement between the predictions and observed distributions. Nonetheless, discrepancies remain, highlighting remaining uncertainties in our understanding of high mass compact binary formation. Our results indicate that no one model completely matches the observed distribution, although the *Standard* remnant mass scheme + *Hobbs kick* and *FryerRapid* scheme + *Bray kick* offer the closest match. The key features which are difficult to match for these model sets are the smaller number of low chirp mass transients and a significant peak around  $\log 1.48$  ( $\sim 30 M_{\odot}$ ). In future, we might consider using a prescription where both the kick and remnant mass are stochastically sampled, similar to Mandel & Müller (2020). Additionally, at the high mass end the physics of pair-instability and pulsational pair-instability systems also need to be taken into account (as in Stevenson et al. 2019). Given that supernovae remnant masses and kicks are interrelated, higher number statistics are needed to fully explore their effects. This should be possible as GW transient catalogs grow in size and completeness.

## ACKNOWLEDGEMENTS

SG and WGJvZ acknowledge support from the University of Auckland. JJE and HFS acknowledge the support of the Marsden Fund Council managed through the Royal Society of New Zealand Te Apārangi. ERS received support from United Kingdom Science and Technology Facilities Council (STFC) grant ST/T000406/1.

## DATA AVAILABILITY

The data underlying this article will be shared on reasonable request to the corresponding author.

## REFERENCES

Abbott B. P., et al., 2016, *Phys. Rev. Lett.*, **116**, 241102  
 Abbott B. P., et al., 2017, *Phys. Rev. Lett.*, **119**, 161101  
 Abbott B., et al., 2019, *Physical Review X*, **9**, 031040  
 Abbott R., et al., 2020a, arXiv e-prints, p. arXiv:2010.14527  
 Abbott R., et al., 2020b, *ApJ*, **896**, L44  
 Abbott R., et al., 2021, *ApJ*, **913**, L7  
 Allen B., Anderson W. G., Brady P. R., Brown D. A., Creighton J. D. E., 2012, *Phys. Rev. D*, **85**, 122006  
 Bailyn C. D., Jain R. K., Coppi P., Orosz J. A., 1998, *ApJ*, **499**, 367  
 Barrett J. W., Gaebel S. M., Neijssel C. J., Vigna-Gómez A., Stevenson S., Berry C. P. L., Farr W. M., Mandel I., 2018, *MNRAS*, **477**, 4685

Belczynski K., Kalogera V., Rasio F. A., Taam R. E., Zezas A., Bulik T., Maccarone T. J., Ivanova N., 2008, *ApJS*, **174**, 223  
 Belczynski K., Bulik T., Mandel I., Sathyaprakash B. S., Zdziarski A. A., Mikołajewska J., 2013, *ApJ*, **764**, 96  
 Belczynski K., Buonanno A., Cantiello M., Fryer C. L., Holz D. E., Mandel I., Miller M. C., Walczak M., 2014, *ApJ*, **789**, 120  
 Belczynski K., Holz D. E., Bulik T., O’Shaughnessy R., 2016, *Nature*, **534**, 512  
 Boco L., Lapi A., Chruslinska M., Donevski D., Sicilia A., Danese L., 2021, *ApJ*, **907**, 110  
 Bray J. C., Eldridge J. J., 2018, *MNRAS*, **480**, 5657  
 Broekgaarden F. S., et al., 2021, arXiv e-prints, p. arXiv:2103.02608  
 Buskirk D., Babiuc-Hamilton M. C., 2019, *EJP*, **40**, 025603  
 Carr B. J., Hawking S. W., 1974, *MNRAS*, **168**, 399  
 Chruslinska M., Nelemans G., Belczynski K., 2019, *MNRAS*, **482**, 5012  
 De Marco O., Izzard R. G., 2017, *Publ. Astron. Soc. Australia*, **34**, e001  
 Eldridge J. J., Stanway E. R., 2016, *MNRAS*, **462**, 3302  
 Eldridge J. J., Tout C. A., 2004, *MNRAS*, **353**, 87  
 Eldridge J. J., Izzard R. G., Tout C. A., 2008, *MNRAS*, **384**, 1109  
 Eldridge J. J., Stanway E. R., Xiao L., McClelland L. A. S., Taylor G., Ng M., Greis S. M. L., Bray J. C., 2017, *PASA*, **34**, e058  
 Eldridge J. J., Stanway E. R., Tang P. N., 2019, *MNRAS*, **482**, 870  
 Finn L. S., 1996, *Phys. Rev. D*, **53**, 2878  
 Fishbach M., Kalogera V., 2021, arXiv e-prints, p. arXiv:2105.06491  
 Fryer C. L., Belczynski K., Wiktorowicz G., Dominik M., Kalogera V., Holz D. E., 2012, *ApJ*, **749**, 91  
 Giacobbo N., Mapelli M., Spera M., 2018, *MNRAS*, **474**, 2959  
 Hobbs G., Lorimer D. R., Lyne A. G., Kramer M., 2005, *MNRAS*, **360**, 974  
 Hogg D. W., 1999, arXiv e-prints, pp astro-ph/9905116  
 Huerta E. A., et al., 2017, *Phys. Rev. D*, **95**, 024038  
 Hurley J. R., Pols O. R., Tout C. A., 2000, *MNRAS*, **315**, 543  
 Ivanova N., et al., 2013, *A&ARv*, **21**, 59  
 Kulkarni S. R., Hut P., McMillan S., 1993, *Nature*, **364**, 421  
 LIGO Scientific Collaboration 2018, LIGO Algorithm Library - LALSuite, Free software (GPL), doi:10.7935/GT1W-FZ16  
 Lipunov V., Gorbvskoy E., Grinshpun V., Vlasenko D., 2021, *MNRAS*, **502**, 1925  
 Maeder A., 1987, *A&A*, **178**, 159  
 Mandel I., Müller B., 2020, *MNRAS*, **499**, 3214  
 Mapelli M., Giacobbo N., Ripamonti E., Spera M., 2017, *MNRAS*, **472**, 2422  
 Marchant P., Langer N., Podsiadlowski P., Tauris T. M., Moriya T. J., 2016, *A&A*, **588**, A50  
 McKernan B., Ford K. E. S., Lyra W., Perets H. B., 2012, *MNRAS*, **425**, 460  
 Özel F., Psaltis D., Narayan R., McClintock J. E., 2010, *ApJ*, **725**, 1918  
 Patton R. A., Sukhbold T., 2020, *MNRAS*, **499**, 2803  
 Peters P. C., 1964, *Physical Review*, **136**, 1224  
 Portegies Zwart S. F., McMillan S. L. W., 2000, *ApJ*, **528**, L17  
 Stanway E. R., Eldridge J. J., 2018, *MNRAS*, **479**, 75  
 Stevenson S., Vigna-Gómez A., Mandel I., Barrett J. W., Neijssel C. J., Perkins D., de Mink S. E., 2017, *Nature Communications*, **8**, 14906  
 Stevenson S., Sampson M., Powell J., Vigna-Gómez A., Neijssel C. J., Szécsi D., Mandel I., 2019, *ApJ*, **882**, 121  
 Tang P. N., Eldridge J. J., Stanway E. R., Bray J. C., 2020, *MNRAS*, **493**, L6  
 Vigna-Gómez A., et al., 2018, *MNRAS*, **481**, 4009  
 Woosley S. E., 2017, *ApJ*, **836**, 244  
 Zevin M., Spera M., Berry C. P. L., Kalogera V., 2020, *ApJ*, **899**, L1  
 Zevin M., et al., 2021, *ApJ*, **910**, 152  
 de Mink S. E., Mandel I., 2016, *MNRAS*, **460**, 3545  
 de Mink S. E., Cantiello M., Langer N., Pols O. R., Brott I., Yoon S. C., 2009, *A&A*, **497**, 243  
 van Zeist W. G. J., Stevance H. F., Eldridge J. J., 2021, *JOSS*, **6**, 2968

This paper has been typeset from a  $\text{\LaTeX}$  file prepared by the author.

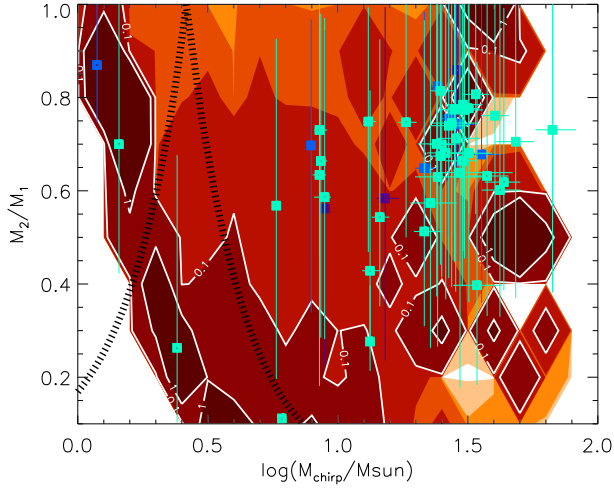


**Figure A1.** Details as in Fig. 3 but here the remnant mass is estimated from the *Standard* remnant mass prescription and the *Bray kick* is used.

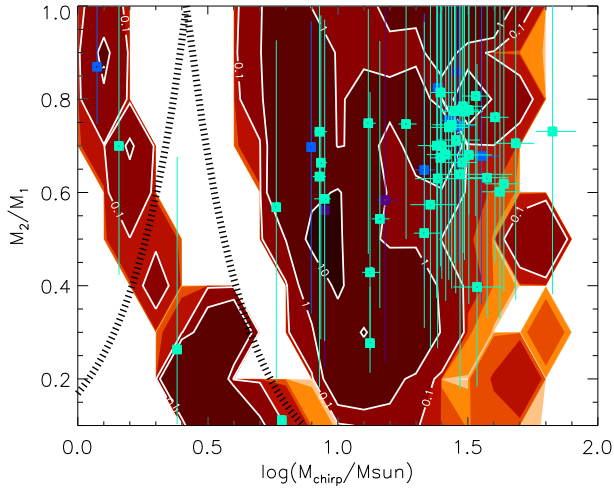


**Figure A2.** Details as in Fig. 3 but here the remnant mass is estimated from the *FryerRapid* remnant mass prescription and the *Hobbs kick* is used.

## APPENDIX A: SUPPLEMENTARY FIGURES FOR GW EVENT DISTRIBUTION IN CHIRP MASS AND MASS RATIO SPACE

This appendix presents the chirp mass distributions associated with the additional supernova kick and remnant mass prescriptions as discussed in the text.

The events vs chirp mass plots in Figs. A1 and A2 complement those in Fig. 3, showing the *Standard* model with the *Bray kick* and the *FryerRapid* in conjunction with *Hobbs kick* scheme respectively. Event rates calculated using the  $M_{\text{CO, final}}$  prescription (Fig. A3) are biased towards the middle of the black hole mass distribution, providing a poor match to the observed data, and also overpredict the rates significantly. Unsurprisingly, event rates calculated using *AlwaysNS* remnant mass prescription (Fig. A4) provide a poor fit to the black hole mass distribution, independent of SN kick prescription. In Fig. A5 we also plot the data shown in Table 1 to assist in its readability.

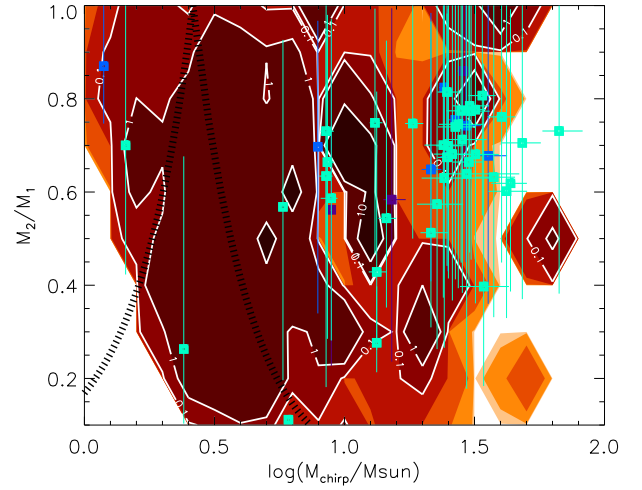
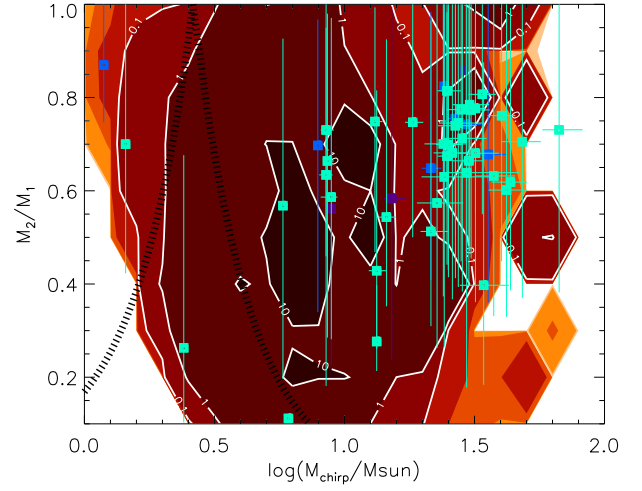


**Figure A3.** Details as in Fig. 3 but here the remnant mass is estimated from the  $M_{\text{CO, final}}$  remnant mass prescription with the upper panels from the *Hobbs kick* and the lower panels from the *Bray kick*.

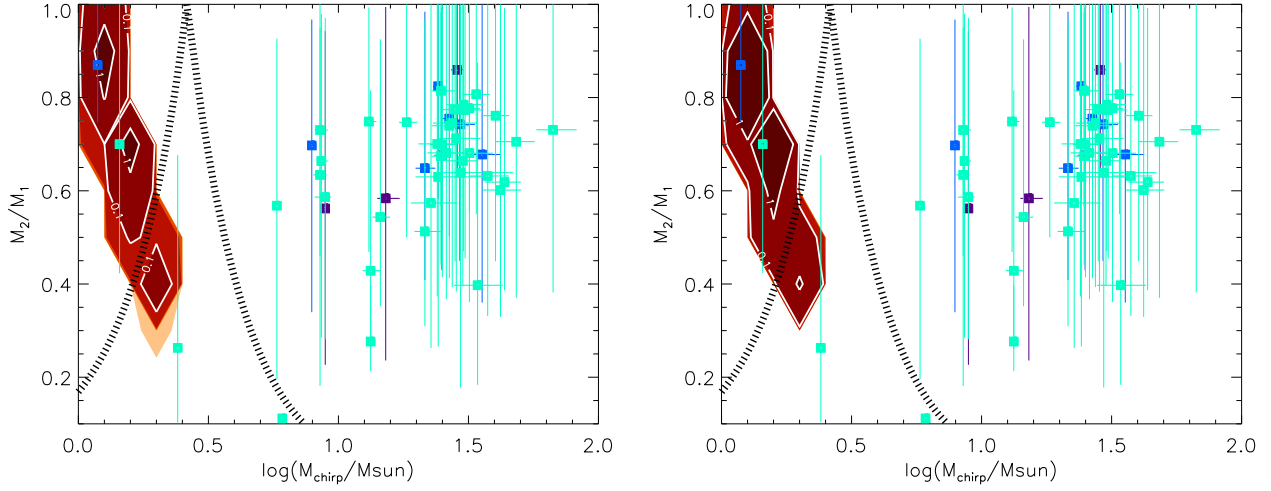


**Figure A4.** Details as in Fig. 3 but here the remnant mass is estimated from the *AlwaysNS* remnant mass prescription with the upper panels from the *Hobbs* kick and the lower panels from the *Bray* kick.

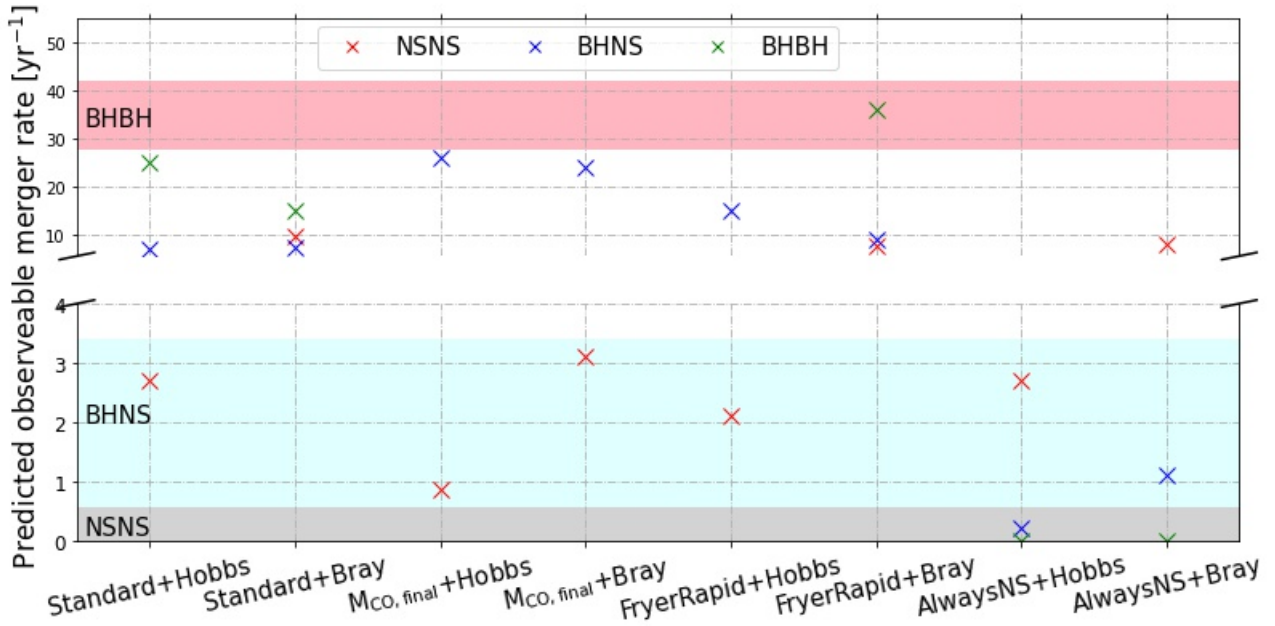


**Figure A5.** To assist in reading, here we plot the predicted detectable merger rates per year as shown in Table 1 by the various schemes. Pink band represents the range of allowed values for BHBH, cyan for BHNS and grey for NSNS merger rates as obtained by LVC O3a, (Abbott et al. 2020a), using their assumptions for the underlying remnant mass distribution (which differs from those explored here). The red crosses are for NSNS, blue for BHNS and green for BHBH merger rates. The BHBH merger rate for  $M_{\text{CO, final}}$  (both kicks) and *FryerRapid* (*Hobbs* kick) are not shown due to their large values. Also the BHBH merger rate for *AlwaysNS* (both kicks) are zero.